Elsevier Editorial System(tm) for Atmospheric Environment

Manuscript Draft

Manuscript Number:

Title: 1951-2017 changes in the frequency of days with visibility higher than 10 km and 20 km in Italy

Article Type: Research Paper

Keywords: Visibility observations; quality checking; variability and trends; atmospheric turbidity; Italy

Corresponding Author: Dr. Veronica Manara,

Corresponding Author's Institution:

First Author: Veronica Manara

Order of Authors: Veronica Manara; Michele Brunetti; Stefania Gilardoni; Tony Christian Landi; Maurizio Maugeri

Abstract: Daily visibility records of the Italian Air Force synoptic stations over the 1951-2017 period have been used to set up a monthly quality/homogeneity checked dataset of fraction of days with visibility higher than or equal to 10 km (fVV10) and 20 km (fVV20) at 12 UTC. This dataset has then been used to calculate regional average fVV10 and fVV20 records for 5 Italian climatic regions. The fVV10 and fVV20 averages show a strong spatial variability with the lowest values in the Po plain, one of the most polluted areas of Europe. In agreement with the results reported in literature for Europe, fVV10 and fVV20 show a positive trend over the whole considered period due to a strong increase starting in the 1980s. Differently, in the previous period, visibility decreases. Moreover, moving from low level areas to mid and high level ones the trends become much weaker, highlighting how the signal decreases with elevation. The analyses performed removing the days with high relative humidity or considering only the clear-sky days show that relative humidity and cloudiness do not have any effect on the observed trends, suggesting that the main driving factor is aerosol load. This hypothesis is supported by the comparison of visibility records with modelled aerosol concentrations, atmospheric optical depth values and emission records. Finally, the trends of fVV10 and fVV20 are in very good agreement with Italian regional records of other variables linked to atmospheric turbidity, like sunshine duration and surface solar radiation.

Research Data Related to this Submission

There are no linked research data sets for this submission. The following reason is given:
Data will be made available on request

Editor
Atmospheric Environment

Bologna, 13th February 2019

Dear Editor,
Attached to this letter you will find the manuscript entitled "1951-2017 changes of days with visibility higher than 10 km and 20 km in Italy", which we are submitting for its publication in Atmospheric Environment. This manuscript has not been submitted elsewhere.
Thank you very much in advance. We are looking forward to hearing good news from you.
Sincerely yours,

Veronica Manara
Institute of Atmospheric Sciences and Climate
ISAC-CNR
via Gobetti 101,
40129, Bologna, Italy
Email: v.manara@isac.cnr.it

1951-2017 changes in the frequency of days with visibility higher than 10 km and 20 km in Italy

Veronica Manara[a] (v.manara@isac.cnr.it)
Michele Brunetti[a] (m.brunetti@isac.cnr.it)
Stefania Gilardoni[a] (s.gilardoni@isac.cnr.it)
Tony Christian Landi[a] (t.landi@isac.cnr.it)
Maurizio Maugeri[b,a] (maurizio.maugeri@unimi.it)
[a] Institute of Atmospheric Sciences and Climate, ISAC-CNR, via Gobetti 101, 40129, Bologna, Italy
[b] Department of Environmental Science and Policy, Università degli Studi di Milano, via Celoria 16, 20133, Milano, Italy;

Corresponding author: Veronica Manara, Institute of Atmospheric Sciences and Climate, ISAC-CNR, via Gobetti 101, 40129, Bologna, Italy (v.manara@isac.cnr.it) http://orcid.org/0000-0001-9652-4228

Abstract

Daily visibility records of the Italian Air Force synoptic stations over the 1951-2017 period have been used to set up a monthly quality/homogeneity checked dataset of fraction of days with visibility higher than or equal to 10 km (fVV10) and 20 km (fVV20) at 12 UTC. This dataset has then been used to calculate regional average fVV10 and fVV20 records for 5 Italian climatic regions. The fVV10 and fVV20 averages show a strong spatial variability with the lowest values in the Po plain, one of the most polluted areas of Europe. In agreement with the results reported in literature for Europe, fVV10 and fVV20 show a positive trend over the whole considered period due to a strong increase starting in the 1980s. Differently, in the previous period, visibility decreases. Moreover, moving from low level areas to mid and high level ones the trends become much weaker, highlighting how the signal decreases with elevation. The analyses performed removing the days with high relative humidity or considering only the clear-sky days show that relative humidity and cloudiness do not have any effect on the observed trends, suggesting that the main driving factor is aerosol load. This hypothesis is supported by the comparison of visibility records with modelled aerosol concentrations, atmospheric optical depth values and emission records. Finally, the trends of fVV10 and fVV20 are in very good agreement with Italian regional

records of other variables linked to atmospheric turbidity, like sunshine duration and surface solar radiation.

Keywords
Visibility observations, quality checking, variability and trends, atmospheric turbidity, Italy

1. Introduction

The World Meteorological Organization (WMO) defines visibility as the greatest distance at which a black object of suitable dimensions (located on the ground) can be seen and recognized when observed against the horizon sky during daylight, or could be seen and recognized during the night if the general illumination were raised to the normal daylight level (WMO, 2008 and references therein). Visibility is reduced by the interaction of light with atmospheric aerosols, which can cause absorption or scattering depending on their size distribution, chemical composition and concentration. They can have natural (e.g., wind-blown dust, volcanic eruptions, wildfires) or anthropogenic (e.g., traffic, energy production, residential heating) origin. Consequently, visibility tends to decrease when air pollutant emissions increase, whereas it is the highest within non-polluted, pristine atmospheres (Sloane, 1982). Visibility is also influenced by meteorological conditions, both in terms of local weather conditions and synoptic weather patterns (Davis, 1991; Sloane, 1983; Van Beelen and Van Delden, 2012), as they can limit or enhance the transport and dispersion of atmospheric aerosols (Founda et al., 2016). Moreover, they influence the aerosol sources and sinks: for example, wind speed promotes the re-suspension of dust particles, temperature and solar radiation trigger photochemistry and favour the production of secondary aerosols, while relative humidity influences aerosols size distribution (Van Beelen and Van Delden, 2012) through hygroscopic growth (Singh et al., 2017) and thus particle ability to diffuse visible light.

The U.S. Environmental Protection Agency (EPA) (EPA, 1979) has identified visibility impairment as the best understood of all environmental effects of air pollution (Watson, 2002). Visibility records can therefore be used to gain useful information on air quality evolution on multi-decadal time scales (Chang et al., 2009) as they generally cover a much wider interval than air quality records (Founda et al., 2016). Besides being a good tracer of air quality, which is strictly connected with human health (Deng et al., 2012; Hu et al., 2017; Zhang et al., 2010), visibility has also an important direct societal impact (Van Oldenborgh et al., 2010). On one side, low visibility impairs all forms of traffic, on the other side, good visibility is a desirable feature of any geographical location (Singh et al., 2017; Zhang et al., 2010). For example, a study at Grand Canyon Park in

USA has shown that visitor frequency in the park has reduced as visibility reduced (Trijonis et al., 1990) and that tourism often depends on good visibility for appreciation of points of interest.

Investigating variability and trends of visibility and the underlying processes, together with the links with other meteorological variables (e.g., surface solar radiation - SSR, sunshine duration - SD, cloudiness, temperature and daily temperature range), can help to better understand the role of aerosols on climate change and to share light on aerosol related phenomena, which are still not adequately represented in climate models (Van Oldenborgh et al., 2010; Vautard et al., 2009).

For all these reasons, visibility is attracting every day more attention in studies focusing on the local, regional, continental and global scale (Boers et al., 2015; Cao et al., 2012; Chang et al., 2009; Doyle and Dorling, 2002; Founda et al., 2016; Hu et al., 2017; Li et al., 2016; Singh et al., 2017; Van Beelen and Van Delden, 2012; Van Oldenborgh et al., 2010; Vautard et al., 2009). These studies report a general increase in visibility (or decrease in the frequency of low-visibility days) after the 1970s-1980s in the United States and Europe, associated with decreasing concentrations of atmospheric aerosols (Hu et al., 2017; Stjern et al., 2011; Vautard et al., 2009). In particular, this increase is found to be less pronounced in less polluted areas (Doyle and Dorling, 2002). Differently, a decreasing tendency of visibility, especially since mid-1990s, is reported for China, both analysing the whole country (-2.1 km per decade from 1990 to 2005, (Che et al., 2007)), and studying single regions (Gao et al., 2011) or megacities (Chang et al., 2009). This is due to the recent rapid economic and industrial development of this country (Deng et al., 2012).

In literature, there are few papers discussing visibility trends in Europe which include also Italian stations (Li et al., 2016; Van Oldenborgh et al., 2010; Vautard et al., 2009). For example, Li et al., (2016) report an increase in visibility after the 1980s in western Europe, while this trend is reported only after the 1990s in eastern Europe, in agreement with the delay of emission reduction in eastern vs. western Europe. Similar results are found by Van Oldenborgh et al., (2010) and Vautard et al., (2009), who report a significant decrease in the number of days with low visibility and highlight a good correlation of this variable with SO_2 emissions and changes in large-scale circulation. However, a paper presenting a comprehensive study of visibility variability and trends in Italy is not yet available and most of visibility data collected at Italian stations are still unexploited.

In this context, this work aims at collecting (Section 2), pre-processing (Section 3) and analysing (Section 4) an extensive database of Italian 1951-2017 visibility records focusing on the fraction of days with visibility higher than or equal to 10 and 20 km. Then, the influence of aerosols on visibility trends is discussed (Section 5) and finally some conclusive remarks are given (Section 6).

2. Data

The data used in this work are Italian Air Force (Aeronautica Militare Italiana – AM) Surface Synoptic Observations (SYNOPs). They were recovered from the AM database (http://clima.meteoam.it/RicercaDati.php) for the 1951-2014 period and from the National Oceanic and Atmospheric Administration website (NOAA - https://www.ncdc.noaa.gov/data-access/quick-links#dsi-3505) for the 2015-2017 period. The latter source allows an easy updating of the records even if it has lower data availability than the former one. The AM database includes records from 168 stations over the entire Italian territory with eight observations per day (see Figure 1 for the spatial distribution of the stations selected after quality/homogeneity checking – Section 3). For each station, together with the data, we recovered also the available metadata, which are useful information during quality/homogeneity checking, allowing to better identify any possible change in the station conditions affecting the quality of the data (Aguilar et al., 2003). For some stations only the coordinates are available while for others, AM provides very detailed metadata (http://www.meteoam.it/page/elenco-stazioni).

We focused on the observations taken at 12 and 15 UTC (i.e. 13 and 16 CET) because they correspond to the day period when relative humidity is at minimum (Cossu et al., 2015; Mooney et al., 2016; Van Beelen and Van Delden, 2012) eliminating the potential influence of morning fogs and biases associated with more difficult visibility estimation during night-time hours (Davis, 1991). In this paper, however, we present only the results concerning 12 UTC as the 15 UTC observation analysis highlights very similar information.

To observe visibility, an operator scans the horizon for predetermined objects (e.g., mountains, islands, churches and buildings) located at known distances. Then, a numerical code is assigned, using the scale recommended by WMO (WMO, 2008 and references therein), where each code is associated to the greatest distance at which a predefined object can be seen and recognized by the naked eye. Moreover, if the observed visibility is between two of known distances (and so associated codes) given in the WMO table, the code for the lower distance is reported. The error of visibility observations increases with distance, and the measurement scale takes this into account by reducing the resolution of the available codes (WMO, 2008). Considering that each station has different reference objects and that the codes have a lower resolution when visibility is high, we have decided to perform the analysis considering the fraction of days with visibility higher than or equal to a certain threshold instead of focusing on mean visibility. Specifically, we have analysed the monthly fraction of days with visibility higher than or equal to 10 km (fVV10 – days with code higher than or equal to 60) and the fraction of days with visibility higher than or equal to 20 km (fVV20 – days with code higher than or equal to 70), where each monthly value is calculated only if at least 80% of data are available. The resulting records range therefore between 0 (if all the

available days have visibility lower than 10 and 20 km, respectively) and 1 (if all the available days have visibility higher than or equal to 10 and 20 km, respectively). The two distance thresholds have been selected with the aim of minimizing the number of records with average value close to 0 or to 1, because these records are less sensitive to changes in visibility.

3. Data pre-processing

3.1 Quality/homogeneity checking procedure

At first, for each series (test series), an independent simulated series is obtained by means of the neighbouring stations (reference series). Specifically, each monthly value is estimated in a leave-one-out approach as weighted median of 11 potential reconstructions (fVV_{test_i}) derived from the 11 reference series with the highest weight among those that are available for the analysed month and have at least 15 years of data in common with the test series. These values are derived under the assumption of the constancy of the ratio between test and reference series by means of the following relation:

$$fVV_{test_i} = fVV_{ref_i} \frac{\overline{fVV_{test}}}{\overline{fVV_{ref_i}}} \qquad (i = 1, \ldots, 11) \qquad (1)$$

where fVV_{ref_i} is the datum of the *i-th* reference series and $\overline{fVV_{test}}$ and $\overline{fVV_{ref_i}}$ are the mean values of the considered month calculated over the common data of the test and the *i-th* reference series.

The weight associated to each reference series in each considered month is calculated as the product of position, elevation, climatology (this one to avoid comparison among stations characterized by very different visibility regimes) and angular weighting functions. The position, elevation and climatology weights are based on Gaussian functions:

$$w = e^{-\left(\frac{\Delta^2}{c}\right)} \qquad (2)$$

with

$$c = \left(\frac{{\Delta_{1/2}}^2}{ln2}\right) \qquad (3)$$

where Δ is the difference between the value of the considered parameter at test and reference station and c is a coefficient that regulates the weight decreasing rate, with $\Delta_{1/2}$ defined as that value of Δ for which the weight is equal to 0.5. For position weight, $\Delta_{1/2}$ is set to 300 km, for elevation weight it is set to 250 m if the test station has elevation lower than or equal to 500 m, otherwise it is set to half of the test station elevation. For climatology weight, $\Delta_{1/2}$ is set to 0.1, with station monthly climatologies calculated over the 15-year period with best data availability. Finally, an angular term is added in order to take into account the anisotropy in spatial distribution of the series (New et al., 2000).

Then, the quality/homogeneity of the series is checked in three steps:

1. Test and corresponding simulated series are visually inspected and the sub-periods with evident inhomogeneities in the test series are eliminated. These inhomogeneities can be due, for example, to periods in which the measures have not been taken adequately, to changes in station location or to permanent or prolonged changes in the area surrounding the station (e.g., construction of large industrial plants or large mobility infrastructures);
2. Single outliers in the series are then eliminated. Specifically, after eliminating inhomogeneous sub-periods in step 1, new simulated series are calculated using the same procedure explained above and a monthly value in the test series is eliminated if the difference (in absolute value) from the corresponding simulated value is higher than a given threshold. This threshold depends on the considered series and month, and it is calculated as $1-\sigma^2$, where σ^2 is the common variance between test and simulated series (to adopt a more stringent or more cautious criterion depending on the representativeness of the simulated series). Moreover, if the threshold is lower than 0.2 or higher than 0.4, it is set to 0.2 or 0.4, respectively. These values are a compromise between the needing of identifying and correcting station outliers and the goal of avoiding removing correct values from the records.
3. The series obtained in this way are then used to calculate new simulated series not affected by outliers and the procedure at step 2 is applied again to the test series obtained from step 1.

Only the series with at least 30 years of data in the period 1951-2017 after this procedure are considered for the following analyses, reducing the database to 97 stations for fVV10 and 77 stations for fVV20 (Figure 1). Considering only the stations included in the final database, the fraction of data eliminated during the quality checks is about 3% for fVV10 and about 11% for fVV20. The fraction of data eliminated for fVV20 is higher because for some stations, especially during the more recent years, METeorological Air Report (METAR) codes are used instead of SYNOP codes for visibility observations. Since the upper bound of METAR codes corresponds to 10 km, when this change occurs the fVV20 series show clear inconsistency. This scale inconsistency has been previously reported in other areas (Chang et al., 2009; Li et al., 2016).

For both datasets, the stations' elevation ranges between 2 m and 3488 m, with 77% of them having an elevation lower than or equal to 500 m (Figure 1 and Figure 2). The mean minimum distance between station pairs is about 44 km for fVV10 and about 51 km for fVV20, while the number of available stations per year is always higher than 43 for fVV10 and 26 for fVV20. The highest data availability is observed from the 1960s to the 1990s (Figure 2).

3.2 Gap-filling procedure

After quality/homogeneity checks, all the missing values in the monthly series included in the final database (Figure 1) are estimated using the same procedure illustrated in Section 3.1 to obtain the simulated series. The procedure is tested with the leave-one-out approach, by considering each available value as missing and estimating it by means of the same procedure used to estimate the real missing values. The resulting mean error (ME) is almost null in all months both for fVV10 and fVV20, suggesting that the method is not affected by systematic errors. The mean absolute error (MAE) is 0.08 and 0.09 for fVV10 and fVV20, respectively, while the corresponding root mean square errors (RMSE) are 0.10 and 0.12.

3.3 Construction of the regional series

For each series, seasonal (March–April-May; June–July-August; September–October-November; December-January-February) and annual (December-November) series are calculated. Then, these series are divided in two groups depending on elevation: stations with elevation lower than or equal to 500 m (75 series for fVV10 and 59 series for fVV20) and stations located at higher elevation (22 series for fVV10 and 18 series for fVV20).

For the stations located at elevation lower than or equal to 500 m, and so representative of low elevation areas, a gridded version (1°x1° resolution) of the database is generated too in order to balance the contribution of those areas with a higher number of stations with those that have a lower station coverage. This gridded version is generated following the technique described in Brunetti et al., (2006), which is based on an Inverse Distance Weighting approach with the addition of an angular term to take into account the anisotropy in spatial distribution of stations. Specifically, a grid point is calculated if there is at least one series at a distance lower than or equal to $d/2$, where d is defined as the mean distance from one grid-point to the next one, calculated over all points of the grid. In this study d is equal to about 140 km. The resulting grid consists of 46 and 39 grid-points for fVV10 and fVV20, respectively (Figure 1). The grid-point series are then divided into northern and southern regions by means of a Principal Component Analysis (Preisendorfer, 1988; Wilks, 1995) and averaged in order to obtain series representative of northern and southern Italy low elevation areas.

Differently, for the series located at elevation higher than 500 m a gridded version is not generated due to the limited number of available records. However, they are divided into three groups: northern Italy stations with elevation between 500 m and 1400 m (8 and 5 series for fVV10 and fVV20, respectively), northern Italy stations with elevation higher than or equal to 1400 m (5 series

for both fVV10 and fVV20) and southern Italy stations with elevation higher than 500 m (9 and 7 series for fVV10 and fVV20, respectively). The series included in each group are then averaged in order to obtain mean series representative, respectively, of the mid and high elevation areas of northern Italy and of the mid-to-high elevation areas of southern Italy. Therefore, for both fVV10 and fVV20 we focus on 5 regional average series: low, mid and high elevation areas for the north and low and mid-to-high elevation areas for the south (L-N, M-N, H-N and L-S, MH-S, respectively).

4. Results

4.1 Station climatologies over the 1951-2017 period

The fVV10 and fVV20 annual and seasonal station mean values over the entire considered period highlight the strong spatial variability of visibility over the Italian territory: they are shown in Figure 3 for winter and summer, with values ranging from 0.17 (Brescia Ghedi - 16088 - winter) to 0.99 (Prizzi – 16434 - summer) for fVV10 and from 0.07 (Torino Caselle – 16059 - winter) to 0.78 (Prizzi – 16434 - summer) for fVV20.

Both in winter and summer, the lowest fVV10 values (Figure 3a and Figure 3b) are in the Po plain (average Po plain fVV10 values in winter and summer are 0.31 and 0.67, respectively and corresponding fVV20 values are 0.13 and 0.27), which has rather continental climate and is one of the most polluted areas of Europe (Bressi et al., 2016; Squizzato et al., 2013). Within the Po plain, visibility progressively increases from the west to the east and from winter to summer, season in which the mid-high elevation sites surrounding it have values that are comparable to the low elevation sites. A good example of the very different dependence of visibility on elevation in winter and summer is given by Torino Caselle (45.22 N; 7.65 E; 301 m) and Torino Bric della Croce (45.03 N; 7.73 E; 710 m): in winter the former site has a strongly lower (0.21) fVV10 mean value than the latter (0.59), whereas in summer the two means are much more similar (0.51 and 0.60, respectively). Outside the Po plain and the surrounding mid and high elevation sites, in summer (Figure 3b) most fVV10 values are over 0.75, with the lowest one in Napoli Capodichino (16289). Sardinia and Sicily stations, together with some costal stations in Apulia and along the Tyrrenian sea, have rather high fVV10 means also in winter, whereas in this season the other stations of the peninsular part of Italy have lower visibility, with values of about 0.60 in the Rome (e.g., 0.62 in Roma Urbe – 16235) and Naples area (e.g., 0.56 in Napoli Capodichino - 16289).

The spatial pattern of fVV20 station mean values (Figure 3c and Figure 3d) highlights the same main features even though in this case the highest values generally concern mid and high elevation stations. In mountain stations fVV10 and fVV20 values are generally rather similar (e.g., Plateau

Rosa – 16052 – 3488 m in winter has a fVV20 normal that is 95% of the corresponding fVV10 normal) as low visibility is often related to foggy conditions producing visibility much lower than 10 km.

4.2 Trend analysis

The mean series of fVV10 and fVV20 for the northern (N) and southern (S) region and for the low (L), mid (M) and high (H) elevation areas are shown in Figure 4 and Figure 5, with corresponding 11-year window, 3-year standard deviation Gaussian low-pass filters. The trends estimated using the Theil-Sen method (Sen, 1968; Theil, 1950) and their significances estimated using the Mann-Kendall non-parametric test (Sneyers, 1992) are shown in Table 1 for three periods (1951-1980, 1981-2017, 1951-2017) and for all the seasons, while the results of trend analysis of the annual records over moving windows with length comprised between 21 and 67 years are shown in Figure 6.

The L-N and L-S fVV10 series (Figure 4 – black lines, Table 1) show a clear positive trend over the whole period under analysis (1951-2017). At annual scale, fVV10 increases of 29% and 7% in the north and in the south, respectively (L-N p-value ≤ 0.01; L-S p-value ≤ 0.05). This increase is observed in all seasons (L-N p-value ≤ 0.01; L-S p-value ≤ 0.1), with the only exception of autumn in the south, where the trend is positive but not significant ($p > 0.1$). The fVV10 positive trend is due to a strong increase starting from about 1980: at annual scale the increase over the 1981-2017 period (brightening period, e.g., Wild, (2016, 2009)) is 38% and 23% in L-N and L-S, respectively (p-value ≤ 0.01) and this increase is significant in all seasons (p-value ≤ 0.01). On the contrary, in the previous period (dimming period. e.g., Wild, (2016, 2009)) visibility decreases. This decrease is significant at annual scale and in all seasons (p-value ≤ 0.01) with the only exception of winter in the north.

It is interesting to underline some regional peculiarities like a stronger trend in L-N than in L-S over the whole considered period, a stronger dimming period decrease in L-S than in L-N and a stronger brightening period increase in L-N than in L-S. Moreover, the brightening period increase is stronger than the previous dimming period decrease in the north while it is much more similar in L-S.

The L-N and L-S fVV20 series (Figure 4 - red lines, Table 1) show a similar behaviour and similar regional peculiarities to that observed for fVV10, even if climatology and intensity of the trends are different.

Moving from low level areas to high level ones, in the north (H-N) (Figure 5 – second column, Table 1) dimming and brightening period trends become weaker for both fVV10 and fVV20. They

are however still significant (p-value ≤ 0.1) at annual scale and in spring and summer. Also northern Italy mid-level areas (M-N) (Figure 5 – first column, Table 1) highlight that signals generally decrease with elevation. The same result is highlighted for southern Italy mid and high level areas (MH-S) showing less pronounced negative and positive trends in the dimming and in the brightening periods than the corresponding low level areas.

It is interesting to underline that both in northern and southern Italy, the strongest dimming and brightening period signals concern summer for both fVV10 and fVV20. It is also worth noticing that the trend signals of different regions and different seasons are not easy to compare as fVV10 and fVV20 become less sensitive to changes in visibility when their average values approach the lower (0) or upper (1) limits.

All the previous results are highlighted also by Figure 6, which gives evidence of the very strong fVV10 and fVV20 signals in the dimming and brightening periods both in L-N and L-S at annual scale. These signals are still present for mid-level sites whereas they become weaker for high level sites.

4.3 Influence of relative humidity (RH) and cloudiness

In order to better understand the impact of high RH days on fVV10 and fVV20 records, we removed from the series included in the final database all observations collected with RH higher than or equal to 90% and we recalculated the regional average records as presented in Sections 3.2 and 3.3. The 11-year window, 3-year standard deviation low-pass filters of these records for low elevation areas (L-N and L-S) are shown in Figure 7 (fVV10 green line, fVV20 orange line), together with the same curves obtained from the full set of observations (fVV10 black line, fVV20 red line). They highlight that high RH observations have a small but significant effect on average fVV10 and fVV20 values, especially in winter and autumn, whereas they do not have any effect on the trends in the dimming and in the brightening periods. Figure 8 (same colours as Figure 7) presents the same curves for mid and high elevation areas (M-N, H-N, MH-S). In this case the differences in fVV10 and fVV20 climatological values are stronger because in mountain areas low visibility is often related to foggy conditions. However, removing the observations with high RH does not alter the dimming and brightening period trends. If we set the threshold to identify high RH observations to 80%, we obtain the same trends in all regions, even though with higher fVV10 and fVV20 climatological values (figure not shown).These results give evidence that fVV10 and fVV20 trends both for northern and southern Italy, do not significantly depend on changes in the fraction of days with high RH.

We investigated visibility trends also focusing on clear-sky days only. These days are here identified as days with total cloud cover (TCC) lower than or equal to 1 okta. Also in this case L-N and L-S curves (blue and grey lines in Figure 7 for fVV10 and fVV20, respectively) show similar features than those obtained for the full dataset. However, especially for fVV20, the dimming and brightening period signals are slightly stronger in all seasons (e.g., at annual scale the increase during the 1981-2017 period is 36% for L-N and 31% for L-S for the full dataset and 52% for L-N and 47% for L-S for the clear-sky dataset). Moving to higher elevations the clear-sky fVV10 records reach the maximum values for H-N and MH-S almost over the whole period, making it very difficult to appreciate any signal except for summer H-N where the dimming and brightening period signals are still present, while M-N curves give evidence of signals much more similar to those obtained considering all the days. Considering the clear-sky M-N and MH-S fVV20 curves, the observed behaviour is comparable to that observed for the full dataset while for H-N the clear-sky fVV20 curves are more similar to the H-N fVV10 ones. Overall, the clear-sky fVV10 and fVV20 show how the dimming and brightening period signals do not significantly depend on cloudiness changes.

It is interesting to underline that removing the days with RH≥90% (RH≥80%) and TCC>1okta from the original series the obtained curves are very similar to those obtained removing only the days with TCC>1okta (results not shown).

5. Discussion

The regional average trends of fVV10 and fVV20 can not be compared with corresponding aerosol concentration trends, because aerosol concentration data are available for a much shorter period than visibility data. Moreover, even for the last 10-15 years, the spatial coverage of aerosol measurements is highly inhomogeneous and large areas of central and southern Italy do not have any records (see e.g. ISPRA, (2014)). Thus, we consider in this discussion modelled aerosol concentrations, atmospheric optical depth (AOD) values and emission data covering a multi-decal period.

Firstly, we compare the spatial pattern of fVV10 and fVV20 average values with that of the modelled aerosol mass concentrations available at hourly resolution for the 2010-2017 period from the European Regional Air Quality production of the Copernicus Atmospheric Monitoring Service (CAMS) initiative (http://www.regional.atmosphere.copernicus.eu/). Specifically, this comparison is performed for each single station using the $PM_{2.5}$ 12UTC daily records of the next neighbour point of the 0.1-degree resolution CAMS grid. Even if the resolution of CAMS grid does not completely capture the orographic details and micrometeorology of some stations, the spatial

distribution of the annual average $PM_{2.5}$ concentrations (Figure 9a) is in agreement with fVV10 means over the common period. Specifically, the Po plain is characterized by the highest concentrations, in agreement with the reported low visibility values (see Figure 3 even if calculated over a different reference period). On the other side, the lowest concentrations are observed over the Alpine chain characterized by high visibility values. The central and southern parts of Italy show lower concentrations than those observed in the Po plain and a lower difference between low and high elevations. However, the urban areas of Rome and Naples show higher values than the surrounding areas, in agreement with relatively low fVV10 values. The scatter plot of fVV10 means versus corresponding $PM_{2.5}$ averages (Figure 9b and Figure 9c) gives further evidence that lower visibility means are associated with higher $PM_{2.5}$ levels. This behaviour is observed both under all-sky (Figure 9b) and clear-sky (Figure 9c) conditions especially for the stations located at low elevations, where the aerosol concentrations are higher. Differently, for the stations located at higher elevation the observed values under all-sky conditions are more connected with the cloudiness variability as already discussed in Section 4.3; in fact, visibility means are always close to 1 once cloud contribution is removed (Figure 9c). Similar results can be obtained also considering fVV20 or using PM_{10} instead of $PM_{2.5}$. Also the temporal evolution of $PM_{2.5}$ (PM_{10}) is in agreement with fVV10 and fVV20 trends because modelled aerosol concentrations decrease in the 2010-2017 period. However, the too short period covered by CAMS data does not allow to go more in depth with this aspect. To investigate the link between visibility and PM concentration trends, we use the latest atmospheric reanalysis of the satellite era produced by NASA's Global Modelling and Assimilation Office (GMAO): Modern-Era Retrospective Analysis for Research and Applications, Version 2 (MERRA-2 - https://gmao.gsfc.nasa.gov/reanalysis/MERRA-2/data_access/ (Gelaro et al., 2017)) with a horizontal resolution of 0.5°x0.625°. Specifically, we investigate the AOD trend (by means of the Sen-Theil method) for each grid-point belonging to the Italian territory available for the 1981-2017 period. The results obtained at annual scale show a negative trend of columnar atmospheric turbidity for all the considered grid-points (Figure 10). Moreover, they show a spatial distribution similar to that of visibility trend (see Figures 4-8 considering the common period) with the strongest variations in the Po plain area (see L-N series), a stronger trend for low than for high elevations (see L-N vs. H-N series) and a trend intensity which decreases from the north to the south (see L-N vs. L-S series). It is also interesting to underline some grid-points over the Apennine chain showing a lower decrease than the surrounding ones, as observed in the visibility series (see L-S vs. MH-S series). In spite of the good agreement with fVV10 and fVV20 trends, it is worth noticing that the AOD is the total column extinction due to all aerosol species. Therefore, this two-dimensional property does not contain information about either

405 the vertical distribution of aerosol extinction or the contribution of any given aerosol species to the
406 extinction at any level of the atmosphere. Thus, even if AOD and visibility observations show the
407 same features, the AOD is an index of air column turbidity, which might be not directly comparable
408 with horizontal visibility at ground level.
409 Finally, on a longer temporal horizon, interesting information can be obtained only from emission
410 data. Specifically, we consider here the Emissions Database for Global Atmospheric Research
411 (EDGAR v4.3.2 - http://edgar.jrc.ec.europa.eu/overview.php?v=432) focusing on the Italian
412 total emission of SO_2, NO_x, NH_3. These species are precursors of secondary aerosols like sulphates
413 and nitrates (Squizzato et al., 2013). Moreover, $PM_{2.5}$ and PM_{10} primary emissions are considered
414 too (Crippa et al., 2018) (Figure 11). The advantage of this dataset is that the emissions are
415 available for the 1970-2012 period (updating to 2015 are in preparation but not yet available at
416 present), thus covering the last years of the dimming period and almost the whole brightening
417 period, allowing a comparison with the visibility records over a longer time scale than the other
418 products discussed above. The emission data highlight the agreement of fVV10 and fVV20 trends,
419 both for the north and south, with the beginning of the decrease of SO_2 emissions corresponding to
420 the beginning of the period of increasing visibility. NO_X starts to decrease from 1995, some years
421 later than SO_2, whereas NH_3 starts to decrease in the period between 1980 and 1995. A similar
422 behaviour is observed for $PM_{2.5}$ and PM_{10} emissions. These patterns are in agreement with the fact
423 that the brightening period fVV10 and fVV20 positive trends become stronger in the 1990s (Figures
424 4-6). EDGAR data set does unfortunately not cover the entire dimming period. However, other
425 emission data show a strong increase in SO_2 emissions over the 1951-1980 period of a factor
426 comprised between 3 and 6 (Mylona, 1996; Smith et al., 2011).
427
428 **6. Conclusions**
429 Daily visibility records of the Italian Air Force synoptic stations over the 1951-2017 period have
430 been used to set up a monthly quality/homogeneity checked dataset of fraction of days with
431 visibility higher than or equal to 10 km (fVV10) and 20 km (fVV20) at 12 UTC. This dataset has
432 then been used to calculate regional average fVV10 and fVV20 records for 5 Italian climatic
433 regions: low, mid and high elevation areas for the northern part of Italy and low and mid-to-high
434 elevation areas for the southern part of Italy (L-N, M-N, H-N and L-S, MH-S, respectively).
435 The fVV10 and fVV20 means over the whole considered period (1951-2017) show a strong spatial
436 variability with the lowest values observed in the Po plain, one of the most polluted areas of
437 Europe.

The L-N and L-S fVV10 series show a positive trend over the whole period under analysis, with the only exception of autumn in the south. This behaviour is due to a strong increase starting in the 1980s. Differently, in the previous period, visibility decreases with the only exception of winter in the north. The L-N and L-S fVV20 series show similar behaviour, even if climatology and intensity of the trends are different. Moving from low level areas to mid and high level ones (M-N, H-N and MH-S) both the fVV10 and fVV20 initial decrease and the following increase become weaker, highlighting how the signal generally decreases with elevation. The analysis performed removing the days with high RH (RH $\geq$ 90%) shows how for low level areas, days with high RH have a small but significant effect on fVV10 and fVV20 climatological values, especially in winter and autumn, whereas they do not have any effect on the trends. The same analysis performed for mid and high elevation areas show stronger differences because in mountain areas low visibility is often related to foggy and cloudy conditions. However, removing the observations with high RH does not alter the long-term trends. Similar results are obtained performing the analysis considering clear-sky days (TCC $\leq$ 1okta) only. Therefore, the strong fVV10 and fVV20 trends observed especially for low-level areas seem to be not significantly influenced by relative humidity and cloudiness and the main driving factor seems to be aerosol load.

Unfortunately, aerosol concentration data are available for a much shorter period than visibility data and for very few sites especially in the southern part of Italy. However, interesting information can be obtained using modelled aerosol concentrations, AOD values s and emission data. In particular, lower visibility means, as those observed in the Po plain or those observed in the main urban sites (e.g., Rome and Naples), are associated with higher $PM_{2.5}$ aerosol concentrations (annual means over the 2010-2017 period - European Regional Air Quality production of CAMS), while higher visibility means are associated with areas where the concentrations are lower (e.g., high elevation sites). Moreover, the strong increase in the fVV10 since the beginning of the 1980s is associated with a strong decrease in the AOD (trend over the 1981-2017 – MERRA2). This link is especially evident in the Po plain and over the Alpine chain. Finally, the decrease in fVV10 and fVV20 (at least since the 1970s) and the following increase show the same features of the total emissions over Italy (EDGAR v4.3.2) of the precursor gases and aerosol primary emissions. In particular, the decrease of SO_2 emissions since 1980, is in agreement with the beginning of the period of increasing visibility, while the decrease of NO_X and NH_3 emissions, which occurred about ten years later, is in agreement with the intensification of fVV10 and fVV20 positive trends observed in the 1990s.

The obtained results are in agreement with those reported in literature for Europe (Founda et al., 2016; Li et al., 2016; Van Oldenborgh et al., 2010; Vautard et al., 2009) which report an increase in

visibility after the 1980s. The observed trends are also in agreement with those reported for the Italian territory for surface solar radiation (SSR) and sunshine duration (SD) by Manara et al., (2017, 2016, 2015). These authors suggested that the variations observed for SSR and SD are due to changes in the transparency of the atmosphere, hypothesizing a significant contribution of aerosols in the clear-sky SSR and SD trends. The results obtained in this paper for fVV10 and fVV20 strengthen this hypothesis, highlighting also some similar regional peculiarities between visibility trends and that of SSR and SD. In fact, visibility series, like clear-sky SSR and SD series, show a stronger trend in the north than in the south over the whole considered period, a stronger dimming period decrease in the south than in the north and a stronger brightening period increase in the north than in the south. Moreover, the brightening period increase is stronger than the previous dimming period decrease in the north while it is slightly lower or comparable in the south.

The observed decrease in the intensity of the trends with elevation is in agreement with the results reported for SSR series in the Piedmont region (Manara et al., 2018). It is interesting to underline that for H-N the visibility trends are significant only during spring and summer probably due to the fact that in these seasons the higher boundary layer causes much more similar aerosol concentrations at low and high elevations (Carbone et al., 2010; Magri et al., 2016). Differently during winter the boundary layer is generally rather low inhibiting the transport of polluted air masses upwards from lower regions by thermal convection (Baltensperger et al., 1991; Carbone et al., 2010; Lugauer et al., 1998) and the high elevation areas have probably been rarely subjected to high aerosol concentrations even in the period of highest aerosol emissions.

Acknowledgements

We acknowledge EDGAR v4.3.2database for the emission inventory data (https://data.europa.eu/doi/10.2904/JRC_DATASET_EDGAR). We are glad to Francesca Soldan who helped us during the preliminary analysis.

References

Aguilar, E., Auer, I., Brunet, M., Peterson, T.C., Wieringa, J., 2003. Guidelines on climate metadata and homogenization. World Clim. Program. Data Monit. WCDMP-No. 53, WMO-TD No. 1186 1186, 50.

Baltensperger, U., Gäggeler, H.W., Jost, D.T., Emmenegger, M., Nägeli, W., 1991. Continuous background aerosol monitoring with the epiphaniometer. Atmos. Environ. Part A, Gen. Top. 25, 629–634. https://doi.org/10.1016/0960-1686(91)90060-K

Boers, R., Van Weele, M., Van Meijgaard, E., Savenije, M., Siebesma, A.P., Bosveld, F., Stammes,

506 P., 2015. Observations and projections of visibility and aerosol optical thickness (1956-2100)
507 in the Netherlands: Impacts of time-varying aerosol composition and hygroscopicity. Environ.
508 Res. Lett. 10, 1–10. https://doi.org/10.1088/1748-9326/10/1/015003
509 Bressi, M., Cavalli, F., Belis, C.A., Putaud, J.P., Fröhlich, R., Martins Dos Santos, S., Petralia, E.,
510 Prévôt, A.S.H., Berico, M., Malaguti, A., Canonaco, F., 2016. Variations in the chemical
511 composition of the submicron aerosol and in the sources of the organic fraction at a regional
512 background site of the Po Valley (Italy). Atmos. Chem. Phys. 16, 12875–12896.
513 https://doi.org/10.5194/acp-16-12875-2016
514 Brunetti, M., Maugeri, M., Monti, F., Nanni, T., 2006. Temperature and precipitation variability in
515 Italy in the last two centuries from homogenised instrumental time series. Int. J. Climatol. 26,
516 345–381. https://doi.org/10.1002/joc.1251
517 Cao, J.J., Wang, Q.Y., Chow, J.C., Watson, J.G., Tie, X.X., Shen, Z.X., Wang, P., An, Z.S., 2012.
518 Impacts of aerosol compositions on visibility impairment in Xi'an, China. Atmos. Environ. 59,
519 559–566. https://doi.org/10.1016/j.atmosenv.2012.05.036
520 Carbone, C., Decesari, S., Mircea, M., Giulianelli, L., Finessi, E., Rinaldi, M., Fuzzi, S., Marinoni,
521 A., Duchi, R., Perrino, C., Sargolini, T., Vardè, M., Sprovieri, F., Gobbi, G.P., Angelini, F.,
522 Facchini, M.C., 2010. Size-resolved aerosol chemical composition over the Italian Peninsula
523 during typical summer and winter conditions. Atmos. Environ. 44, 5269–5278.
524 https://doi.org/10.1016/j.atmosenv.2010.08.008
525 Chang, D., Song, Y., Liu, B., 2009. Visibility trends in six megacities in China 1973-2007. Atmos.
526 Res. 94, 161–167. https://doi.org/10.1016/j.atmosres.2009.05.006
527 Che, H., Zhang, X., Li, Y., Zhou, Z., Qu, J.J., 2007. Horizontal visibility trends in China 1981-
528 2005. Geophys. Res. Lett. 34, 1–5. https://doi.org/10.1029/2007GL031450
529 Cossu, F., Hocke, K., Mätzler, C., 2015. A 10-year cloud fraction climatology of liquid water
530 clouds over Bern observed by a ground-based microwave radiometer. Remote Sens. 7, 7768–
531 7784. https://doi.org/10.3390/rs70607768
532 Crippa, M., Guizzardi, D., Muntean, M., Schaaf, E., Dentener, F., Van Aardenne, J.A., Monni, S.,
533 Doering, U., Olivier, J.G.J., Pagliari, Va., Janssens-Maenhout, G., 2018. Gridded emissions of
534 air pollutants for the period 1970-2012 within EDGAR v4.3.2. Earth Syst. Sci. Data 10, 1987–
535 2013.
536 Davis, R.E., 1991. A synoptic climatological analysis of winter visibility trends in the mideastern
537 United States. Atmos. Environ. 25B, 165–175. https://doi.org/10.1016/0957-1272/91
538 Deng, J., Du, K., Wang, K., Yuan, C.S., Zhao, J., 2012. Long-term atmospheric visibility trend in
539 Southeast China, 1973-2010. Atmos. Environ. 59, 11–21.

https://doi.org/10.1016/j.atmosenv.2012.05.023
Doyle, M., Dorling, S., 2002. Visibility trends in the UK 1950-1997. Atmos. Environ. 36, 3161–3172. https://doi.org/10.1016/S1352-2310(02)00248-0
EPA, 1979. Protecting Visibility: An EPA Report to Congress.
Founda, D., Kazadzis, S., Mihalopoulos, N., Gerasopoulos, E., Lianou, M., Raptis, P.I., 2016. Long-term visibility variation in Athens (1931-2013): A proxy for local and regional atmospheric aerosol loads. Atmos. Chem. Phys. 16, 11219–11236. https://doi.org/10.5194/acp-16-11219-2016
Gao, L., Jia, G., Zhang, R., Che, H., Fu, C., Wang, T., Zhang, M., Jiang, H., Yan, P., 2011. Visual range trends in the Yangtze River Delta Region of China, 1981-2005. J. Air Waste Manag. Assoc. 61, 843–849. https://doi.org/10.3155/1047-3289.61.8.843
Gelaro, R., McCarty, W., Suárez, M.J., Todling, R., Molod, A., Takacs, L., Randles, C.A., Darmenov, A., Bosilovich, M.G., Reichle, R., Wargan, K., Coy, L., Cullather, R., Draper, C., Akella, S., Buchard, V., Conaty, A., da Silva, A.M., Gu, W., Kim, G.K., Koster, R., Lucchesi, R., Merkova, D., Nielsen, J.E., Partyka, G., Pawson, S., Putman, W., Rienecker, M., Schubert, S.D., Sienkiewicz, M., Zhao, B., 2017. The Modern-Era Retrospective Analysis for Research and Applications, Version 2 (MERRA-2). J. Clim. 30, 5419–5454. https://doi.org/10.1175/JCLI-D-16-0758.1
Hu, Y., Yao, L., Cheng, Z., Wang, Y., 2017. Long-term atmospheric visibility trends in megacities of China, India and the United States. Environ. Res. 159, 466–473. https://doi.org/10.1016/j.envres.2017.08.018
ISPRA, 2014. Analisi dei trend dei principali inquinanti atmosferici in Italia 2003-2012.
Li, C., Martin, R. V., Boys, B.L., Van Donkelaar, A., Ruzzante, S., 2016. Evaluation and application of multi-decadal visibility data for trend analysis of atmospheric haze. Atmos. Chem. Phys. 16, 2435–2457. https://doi.org/10.5194/acp-16-2435-2016
Lugauer, M., Baltensperger, U., Furger, M., Gäggeler, H.W., Jost, D.T., Schwikowski, M., Wanner, H., 1998. Aerosol transport to the high Alpine sites Jungfraujoch (3454 m asl) and Colle Gnifetti (4452 m asl). Tellus, Ser. B Chem. Phys. Meteorol. 50, 76–92. https://doi.org/10.3402/tellusb.v50i1.16026
Magri, T., Angelino, E., Grosa, M., Lazzeri, P., Marson, G., De Martini, A., Piccolroaz, S., Zublena, M., 2016. Riscaldamento domestico a legna e qualità dell'aria nelle regioni dell'arco alpino. ISPRA 68/2016.
Manara, V., Bassi, M., Brunetti, M., Cagnazzi, B., Maugeri, M., 2018. 1990–2016 surface solar radiation variability and trend over the Piedmont region (northwest Italy). Theor. Appl.

574 Climatol. in press. https://doi.org/10.1007/s00704-018-2521-6
575 Manara, V., Beltrano, M.C., Brunetti, M., Maugeri, M., Sanchez-Lorenzo, A., Simolo, C., Sorrenti,
576 S., 2015. Sunshine duration variability and trends in Italy from homogenized instrumental time
577 series (1936-2013). J. Geophys. Res. Atmos. 120, 3622–3641.
578 https://doi.org/10.1002/2014JD022560
579 Manara, V., Brunetti, M., Celozzi, A., Maugeri, M., Sanchez-Lorenzo, A., Wild, M., 2016.
580 Detection of dimming/brightening in Italy from homogenized all-sky and clear-sky surface
581 solar radiation records and underlying causes (1959-2013). Atmos. Chem. Phys. 16, 11145–
582 11161. https://doi.org/10.5194/acp-16-11145-2016
583 Manara, V., Brunetti, M., Maugeri, M., Sanchez-Lorenzo, A., Wild, M., 2017. Sunshine duration
584 and global radiation trends in Italy (1959-2013): To what extent do they agree? J. Geophys.
585 Res. 122, 4312–4331. https://doi.org/10.1002/2016JD026374
586 Mooney, P.A., Mulligan, F.J., Broderick, C., 2016. Diurnal cycle of precipitation over the British
587 Isles in a 0.44° WRF multiphysics regional climate ensemble over the period 1990–1995.
588 Clim. Dyn. 47, 3281–3300. https://doi.org/10.1007/s00382-016-3026-6
589 Mylona, S., 1996. Sulphur dioxide emissions in Europe 1880-1991 and their effect on sulphur
590 concentrations and depositions. Tellus 48B, 662–689.
591 New, M., Hulme, M., Jones, P., 2000. Representing twentieth-century space-time climate
592 variability. Part II: Development of 1901-96 monthly grids of terrestrial surface climate. J.
593 Clim. 13, 2217–2238. https://doi.org/10.1175/1520-0442(2000)013<2217:RTCSTC>2.0.CO;2
594 Preisendorfer, R.W., 1988. Principal component analysis in meteorology and oceanography. New
595 York. https://doi.org/10.1029/JD093iD09p10815
596 Sen, P.K., 1968. Estimates of the Regression Coefficient Based on Kendall's Tau. J. Am. Stat.
597 Assoc. 63, 1379–1389. https://doi.org/10.1080/01621459.1968.10480934
598 Singh, A., Bloss, W.J., Pope, F.D., 2017. 60 years of UK visibility measurements: Impact of
599 meteorology and atmospheric pollutants on visibility. Atmos. Chem. Phys. 17, 2085–2101.
600 https://doi.org/10.5194/acp-17-2085-2017
601 Sloane, C.S., 1983. Summertime visibility declines: Meteorological influences. Atmos. Environ. 17,
602 763–774. https://doi.org/10.1016/0004-6981/83/040763-12
603 Sloane, C.S., 1982. Visibility trends - I. Methods of analysis. Atmos. Environ. 16, 41–51.
604 https://doi.org/0004-6981/82/010041-11
605 Smith, S.J., Van Aardenne, J., Klimont, Z., Andres, R.J., Volke, A., Delgado Arias, S., 2011.
606 Anthropogenic sulfur dioxide emissions: 1850-2005. Atmos. Chem. Phys. 11, 1101–1116.
607 https://doi.org/10.5194/acp-11-1101-2011

Sneyers, R., 1992. On the use of statistical analysis for the objective determination of climate change. Meteorol. Zeitschrift 1, 247–256.

Squizzato, S., Masiol, M., Brunelli, A., Pistollato, S., Tarabotti, E., Rampazzo, G., Pavoni, B., 2013. Factors determining the formation of secondary inorganic aerosol: A case study in the Po Valley (Italy). Atmos. Chem. Phys. 13, 1927–1939. https://doi.org/10.5194/acp-13-1927-2013

Stjern, C.W., Stohl, A., Kristjánsson, J.E., 2011. Have aerosols affected trends in visibility and precipitation in Europe? J. Geophys. Res. Atmos. 116, 1–15. https://doi.org/10.1029/2010JD014603

Theil, H., 1950. A rank-invariant method of linear and polynomical regression analysis, in: Proceedings of the Royal Academy of Sciences. pp. 386–392.

Trijonis, J.C., Malm, W.C., Pitchford, M., White, W.H., Charlson, R., Husar, R., 1990. Visibility existing and historical conditions - causes and effects, national acid precipitation assessment program (NAPAP), Report 24. Washington, D. C.

Van Beelen, A.J., Van Delden, A., 2012. Cleaner air brings better views, more sunshine and warmer summer days in the Netherlands. Weather 67, 21–25. https://doi.org/10.1002/wea.854

Van Oldenborgh, G.J., Yiou, P., Vautard, R., 2010. On the roles of circulation and aerosols in the decline of mist and dense fog in Europe over the last 30 years. Atmos. Chem. Phys. 10, 4597–4609. https://doi.org/10.5194/acp-10-4597-2010

Vautard, R., Yiou, P., Van Oldenborgh, G.J., 2009. Decline of fog, mist and haze in Europe over the past 30 years. Nat. Geosci. 2, 115–119. https://doi.org/10.1038/ngeo414

Watson, J.G., 2002. Visibility: Science and Regulation - Critical Review. J. Air Waste Manag. Assoc. 52, 628–713.

Wild, M., 2016. Decadal changes in radiative fluxes at land and ocean surfaces and their relevance for global warming. Wiley Interdiscip. Rev. Clim. Chang. 7, 91–107. https://doi.org/10.1002/wcc.372

Wild, M., 2009. Global dimming and brightening: A review. J. Geophys. Res. 114, D00D16. https://doi.org/10.1029/2008JD011470

Wilks, D.S., 1995. Statistical methods in the atmospheric sciences. Int. Geophys. Ser. 59, 464. https://doi.org/10.1007/s13398-014-0173-7.2

WMO, 2008. Measurement of Visibility. Guid. to Meteorol. Instruments Methods Obs. I.9-1-I.9-14.

Zhang, Q.H., Zhang, J.P., Xue, H.W., 2010. The challenge of improving visibility in Beijing. Atmos. Chem. Phys. 10, 7821–7827. https://doi.org/10.5194/acp-10-7821-2010

EDGAR v.4.3.2 dataset https://data.europa.eu/doi/10.2904/JRC_DATASET_EDGAR

642

		Year	Winter	Spring	Summer	Autumn
L-N fVV10	1951-1980	**-0.12±0.02**	-	**-0.12±0.04**	**-0.23±0.04**	**-0.16±0.02**
	1981-2017	**0.38±0.01**	**0.30±0.03**	**0.38±0.02**	**0.46±0.03**	**0.38±0.02**
	1951-2017	**0.29±0.04**	**0.27±0.03**	**0.27±0.04**	**0.35±0.07**	**0.27±0.04**
L-S fVV10	1951-1980	**-0.22±0.02**	**-0.12±0.02**	**-0.20±0.02**	**-0.28±0.02**	**-0.21±0.03**
	1981-2017	**0.23±0.01**	**0.18±0.02**	**0.24±0.02**	**0.30±0.03**	**0.19±0.01**
	1951-2017	**0.07±0.03**	0.04±0.02	**0.07±0.03**	**0.12±0.04**	+
M-N fVV10	1951-1980	**-0.19±0.01**	**-0.14±0.02**	**-0.20±0.03**	**-0.27±0.03**	**-0.17±0.02**
	1981-2017	**0.30±0.02**	**0.15±0.03**	**0.36±0.03**	**0.37±0.03**	**0.25±0.03**
	1951-2017	**0.17±0.03**	**0.11±0.03**	**0.18±0.05**	**0.23±0.05**	**0.12±0.04**
H-N fVV10	1951-1980	**-0.07±0.02**	-	**-0.10±0.04**	**-0.13±0.03**	+
	1981-2017	**0.06±0.02**	-	**0.14±0.03**	**0.13±0.03**	+
	1951-2017	**0.05±0.02**	+	**0.07±0.03**	**0.10±0.03**	+
MH-S fVV10	1951-1980	-0.03±0.02	+	-0.06±0.03	**-0.04±0.02**	-
	1981-2017	**0.06±0.01**	+	**0.06±0.02**	**0.05±0.01**	**0.06±0.02**
	1951-2017	**0.07±0.01**	**0.08±0.03**	**0.08±0.02**	**0.05±0.01**	**0.06±0.02**
L-N fVV20	1951-1980	-	0.04±0.02	-	**-0.06±0.02**	-
	1981-2017	**0.36±0.02**	**0.24±0.04**	**0.35±0.04**	**0.53±0.03**	**0.33±0.03**
	1951-2017	**0.30±0.03**	**0.24±0.02**	**0.28±0.04**	**0.40±0.06**	**0.27±0.03**
L-S fVV20	1951-1980	**-0.10±0.02**	0.05±0.03	**-0.07±0.02**	**-0.23±0.03**	**-0.09±0.03**
	1981-2017	**0.31±0.03**	**0.17±0.03**	**0.28±0.04**	**0.49±0.04**	**0.26±0.03**
	1951-2017	**0.11±0.04**	**0.07±0.02**	**0.10±0.04**	**0.24±0.06**	**0.10±0.04**
M-N fVV20	1951-1980	-0.05±0.02	-	-	**-0.12±0.04**	+
	1981-2017	**0.32±0.02**	**0.12±0.04**	**0.36±0.03**	**0.53±0.03**	**0.26±0.03**
	1951-2017	**0.24±0.04**	**0.18±0.02**	**0.22±0.04**	**0.33±0.06**	**0.18±0.03**
H-N fVV20	1951-1980	**-0.08±0.02**	-	**-0.13±0.05**	**-0.13±0.03**	+
	1981-2017	**0.06±0.02**	-	**0.16±0.04**	**0.17±0.04**	-
	1951-2017	**0.04±0.02**	+	**0.07±0.04**	**0.10±0.04**	-
MH-S fVV20	1951-1980	**-0.07±0.03**	-	-	**-0.15±0.06**	**-0.07±0.04**
	1981-2017	**0.10±0.04**	+	+	**0.28±0.05**	**0.08±0.05**
	1951-2017	-	+	+	+	-

643 **Table 1**

644

Table Captions

Table 1. Trends expressed as fVV10 and fVV20 variations over three periods (1951-1980; 1981-2017; 1951-2017) provided together with an estimation of their standard deviations (half widths of 68% confidence intervals). Values are shown in roman for significance level $0.05<p\leq0.1$ and in bold for a significance level $p\leq0.05$. For non-significant trends, only the sign of the slope is given. The trends are estimated with the Theil-Sen method while the significance of the trends is evaluated with the Mann-Kendall non-parametric test.

Figure Captions

Figure 1. (a) Spatial distribution of the 97 stations included in the final database (they are the sites with more than 30 years of data after quality/homogeneity checking – see Section 3) for fVV10; (b) Spatial distribution of the 77 stations included in the final database for fVV20. The stations with elevation lower than or equal to 500 m are represented with a circle (Low elevation) while those located at higher elevation are represented with a triangle (Mid-to-high elevation). A larger symbol is used for the series with more than 45 years of available data. For each station the last digits of the WMO code are reported too. The red symbols (stars for the northern part of Italy and crosses for the southern part of Italy) represent the grid-points used to calculate the low elevation regional series (see Section 3.3). The panels also show the orography of the region.

Figure 2. (a) Number of fVV10 records for three elevation ranges; (b) Number of fVV10 records per year considering the entire dataset (solid line), only the stations with elevation lower than or equal to 500 m (Low elevation stations – dashed line) and only the stations with elevation higher than 500 m (Mid-to-high elevation stations – dotted line); (c) and (d) as (a) and (b) but for fVV20.

Figure 3. (a) Winter mean fVV10 values over the 1951-2017 period; (b) Summer mean fVV10 values over the 1951-2017 period; (c) and (d) as (a) and (b) but for fVV20. The stations with elevation lower than or equal to 500 m are represented with a circle while the stations with elevation higher than 500 m are represented with a triangle.

Figure 4. Annual and seasonal L-N (left column) and L-S (right column) fVV10 (thick black lines) and fVV20 (thick red lines) series plotted together with corresponding 11-year window, 3-year standard deviation Gaussian low-pass filters (thin lines).

Figure 5. Annual and seasonal M-N (first column), H-N (second column) and MH-S (third column) fVV10 (thick black lines) and fVV20 (thick red lines) series plotted together with corresponding 11-year window, 3-year standard deviation Gaussian low-pass filters (thin lines).

Figure 6. L-N, M-N, H-N, L-S and MH-S annual fVV10 (left column) and fVV20 (right column) running trend analysis. The y and x axes represent the length and the first year of the period under analysis, respectively, while the coloured pixels show the Theil-Sen trend expressed as variations per decade with a Mann-Kendall significance level $p \leq 0.05$ (large squares) and $p > 0.05$ (small squares).

687

688 *Figure 7. Annual and seasonal 11-year window, 3-year standard deviation Gaussian low-pass*
689 *filters for L-N (left column) and L-S (right column) fVV10 and fVV20 series. Black and res lines are*
690 *for fVV10 and fVV20 using all available days, green and orange lines are for fVV10 and fVV20*
691 *removing the days with RH ≥ 90% and blue and grey lines are for fVV10 and fVV20 selecting only*
692 *the days with TCC ≤ 1okta.*

693

694 *Figure 8. Annual and seasonal 11-year window, 3-year standard deviation Gaussian low-pass*
695 *filters for M-N (first column), H-N (second column) and MH-S (third column) fVV10 and fVV20*
696 *series. Black and res lines are for fVV10 and fVV20 using all available days, green and orange*
697 *lines are for fVV10 and fVV20 removing the days with RH ≥ 90% and blue and grey lines are for*
698 *fVV10 and fVV20 selecting only the days with TCC ≤ 1okta.*

699

700 *Figure 9. (a) $PM_{2.5}$ annual average concentrations calculated over the 2010-2017 period in*
701 *correspondence with the stations reported in Figure 1; (b) fVV10 annual average in relation to*
702 *$PM_{2.5}$ annual average concentrations for the 2010-2017 period; (c) as panel (b) but considering*
703 *only the days with TCC ≤ 1okta. The aerosol concentrations are calculated by the Ensemble*
704 *modelling, provided by the Copernicus Atmospheric Monitoring Service (CAMS) initiative.*

705

706 *Figure 10. MERRA-2 (Modern-Era Retrospective Analysis for Research and Applications, Version*
707 *2) annual aerosol optical depth trends (expressed as variation per decade) for the grid-points*
708 *belonging to the Italian territory over the 1981-2017 period. The trends are estimated with the*
709 *Theil-Sen method.*

710

711 *Figure 11. (a) Total annual Italian emissions of SO_2 (red line), NO_x (blue line) and NH_3 (orange*
712 *line). The data come from the Emissions Database for Global Atmospheric Research (EDGAR*
713 *v4.3.2); (b) as panel (a) but for $PM_{2.5}$ (red line) and PM_{10} (black line).*

Figure 1

Click here to download high resolution image

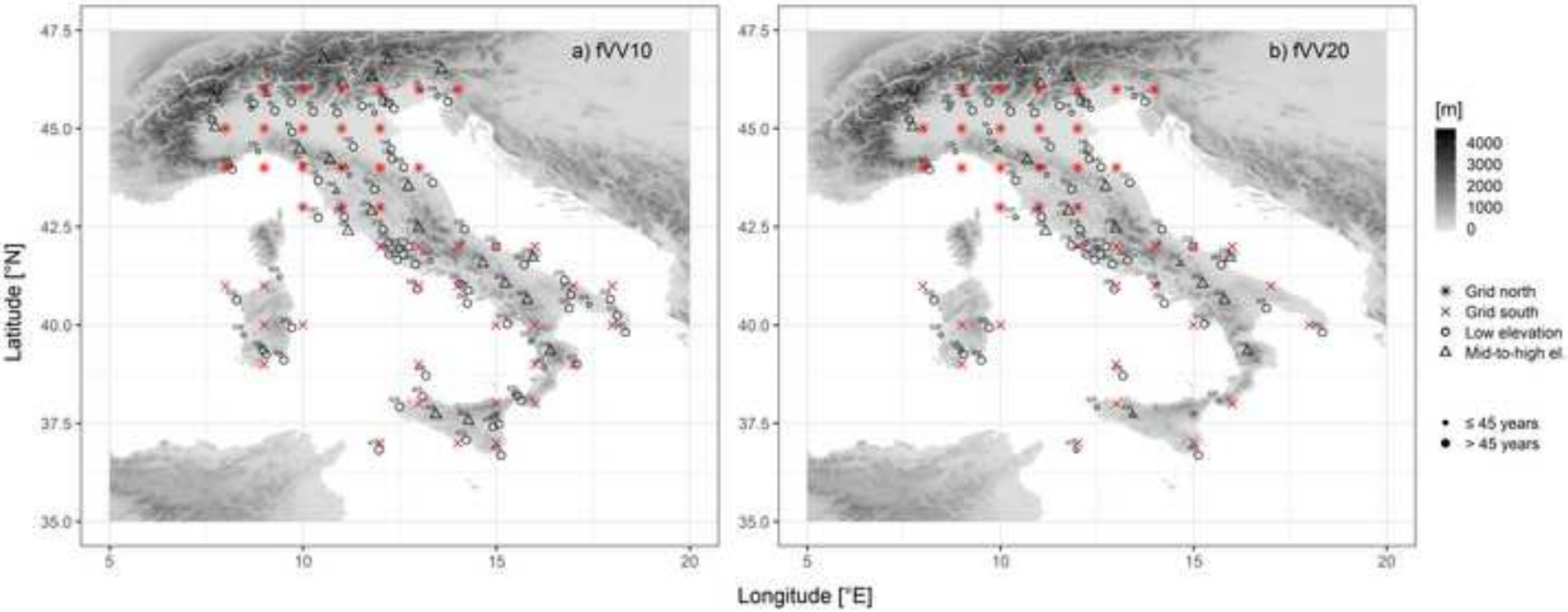

Figure 2

Click here to download high resolution image

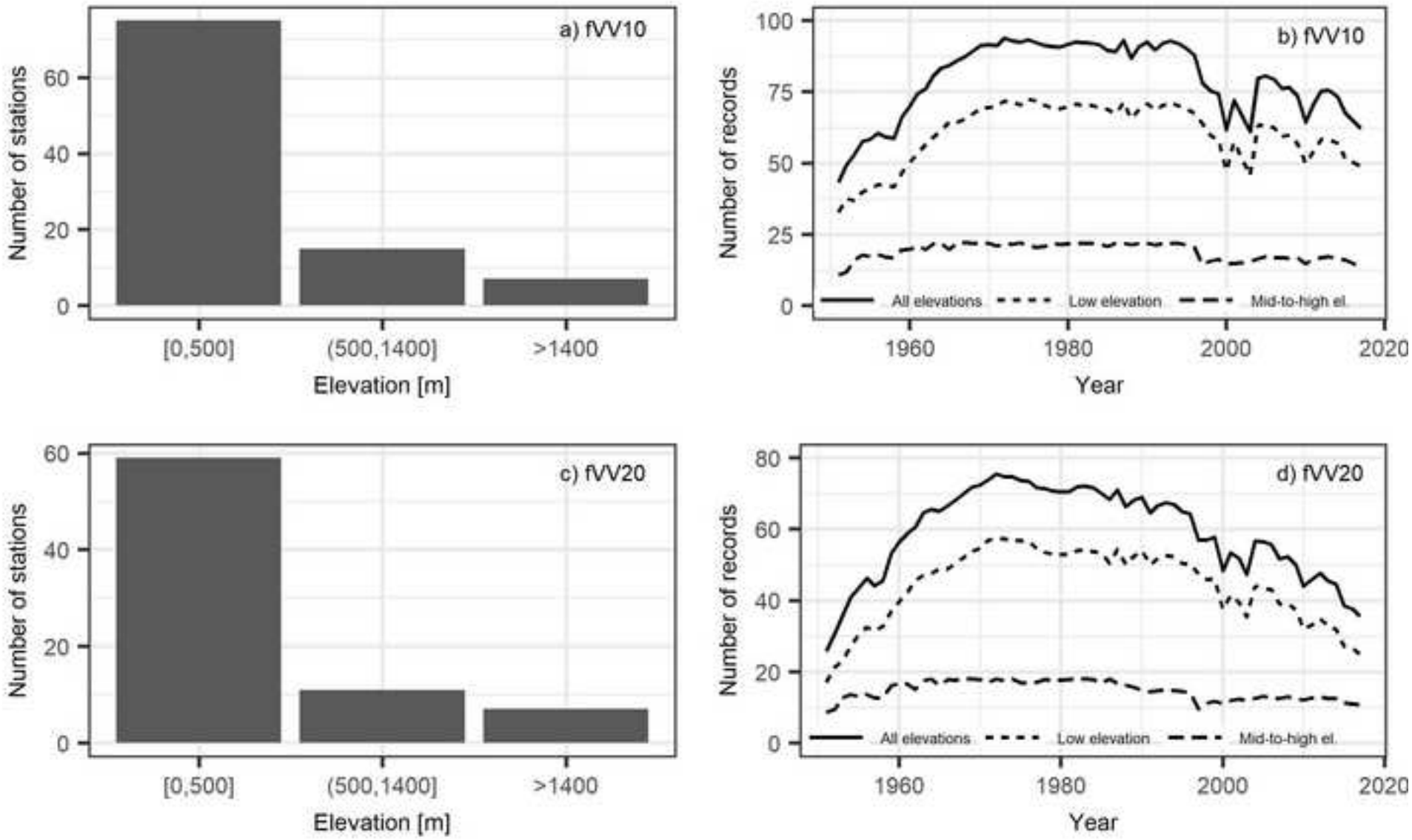

Figure 3

Click here to download high resolution image

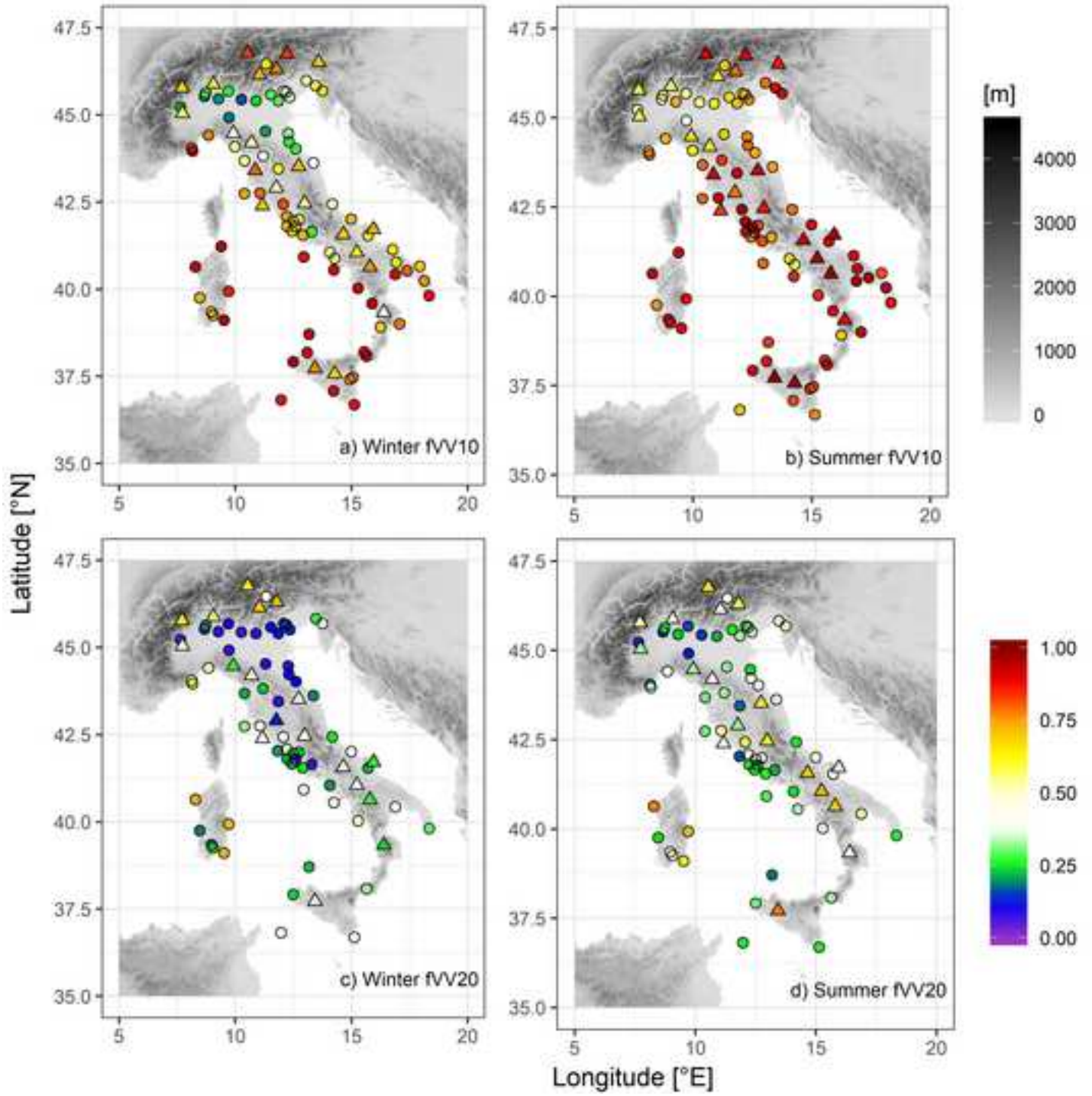

Figure 4

Click here to download high resolution image

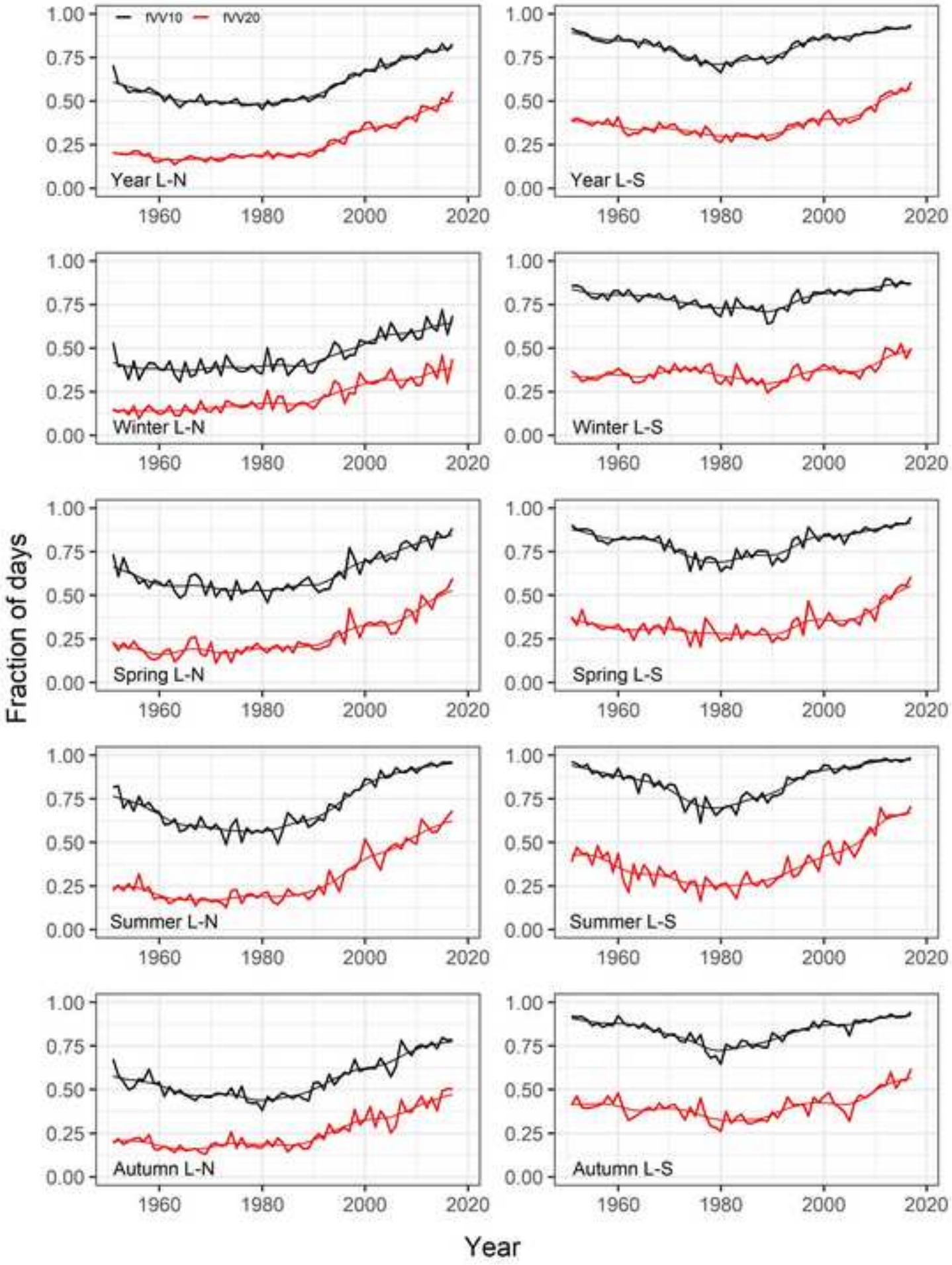

Figure 5

Click here to download high resolution image

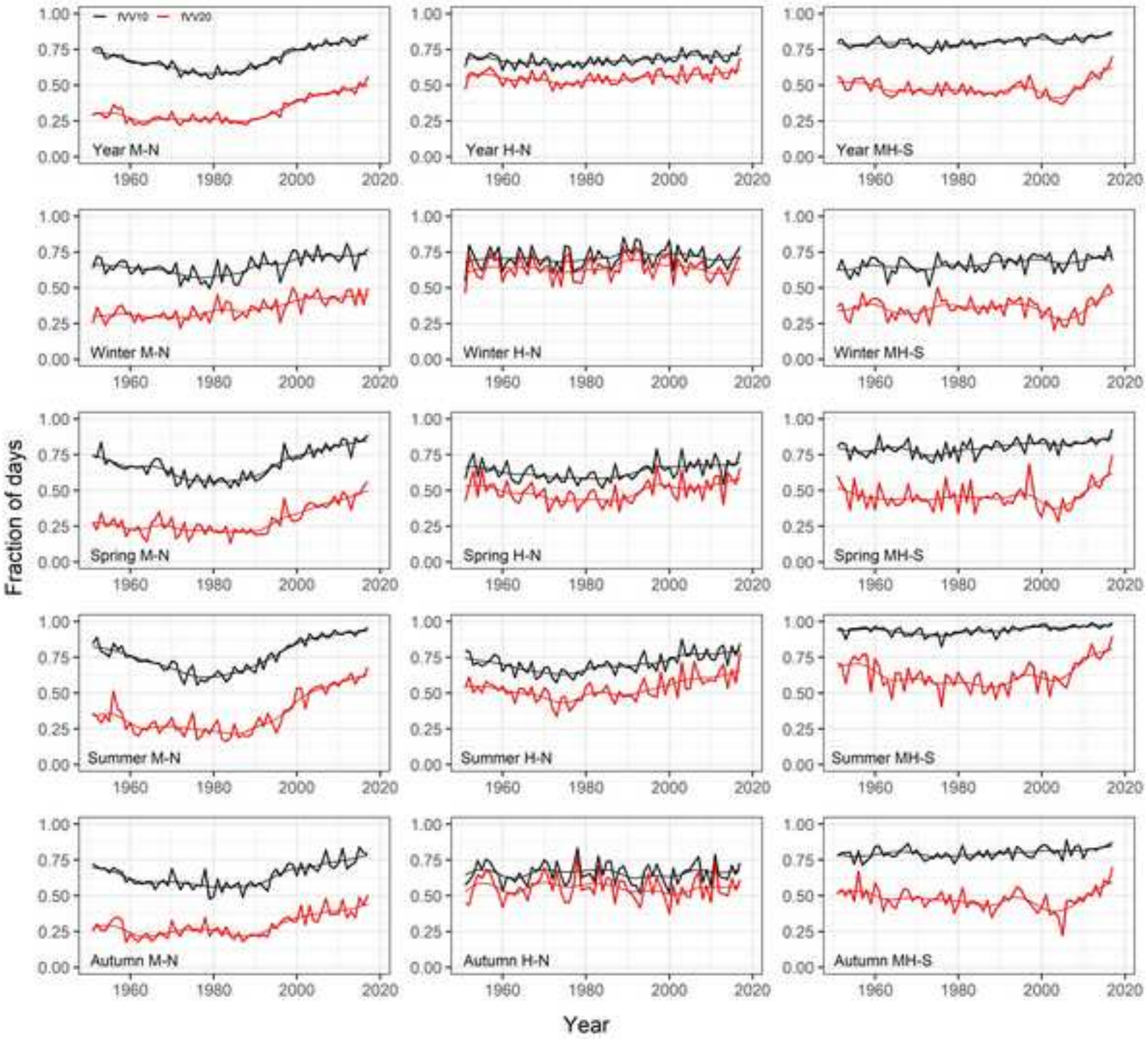

Figure 6

Click here to download high resolution image

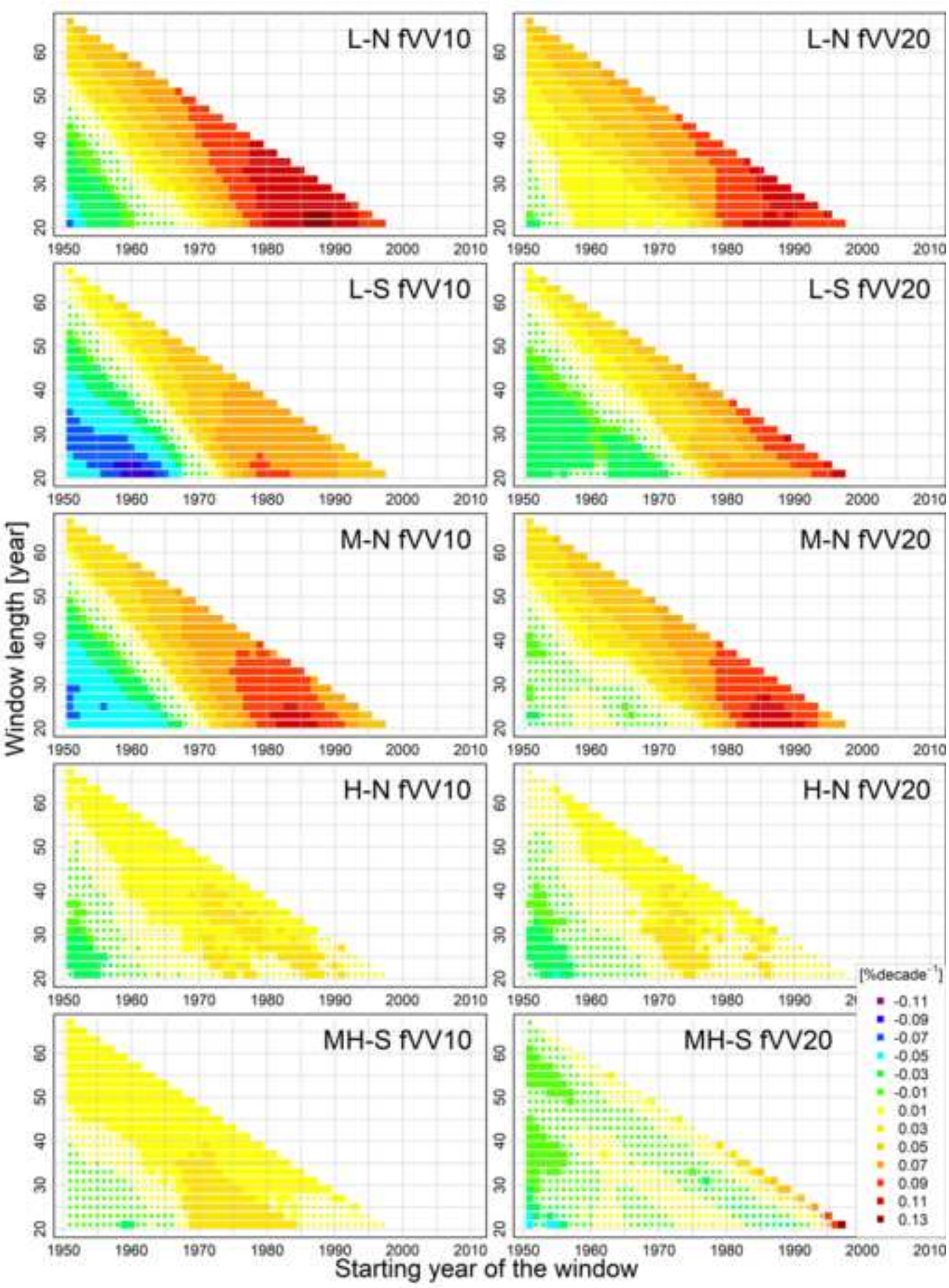

Figure 7

Click here to download high resolution image

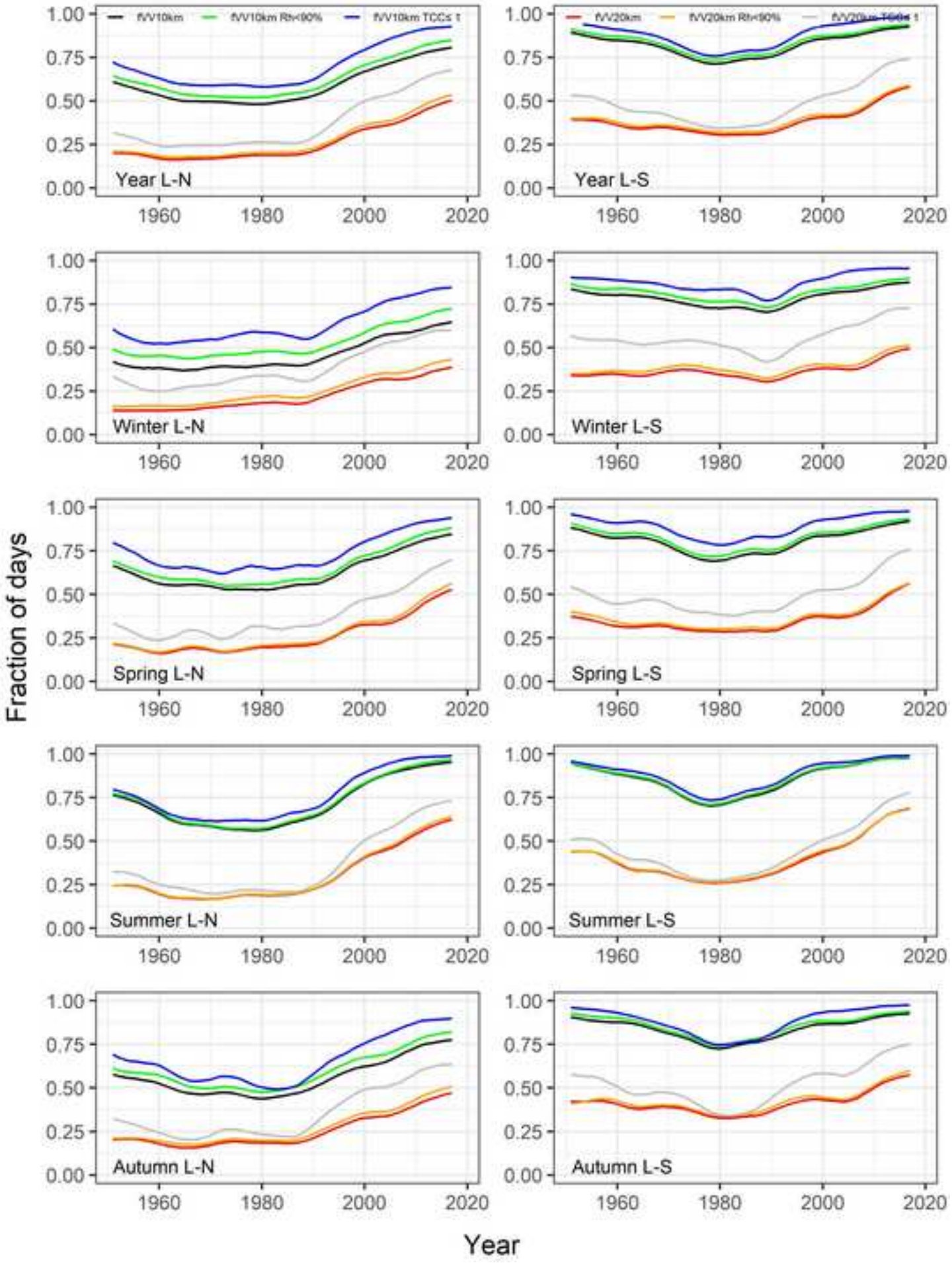

Figure 8

Click here to download high resolution image

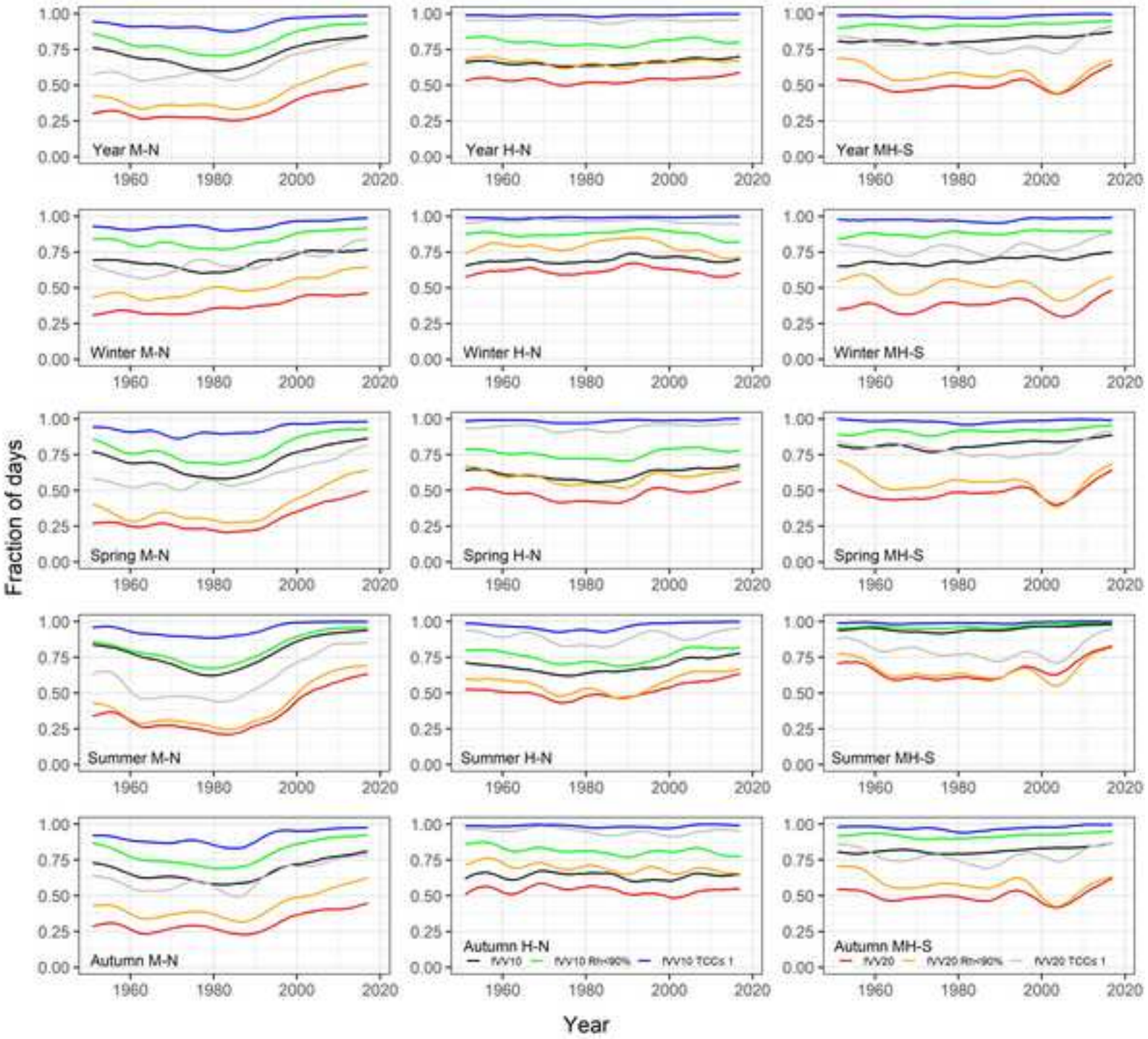

Figure 9

Click here to download high resolution image

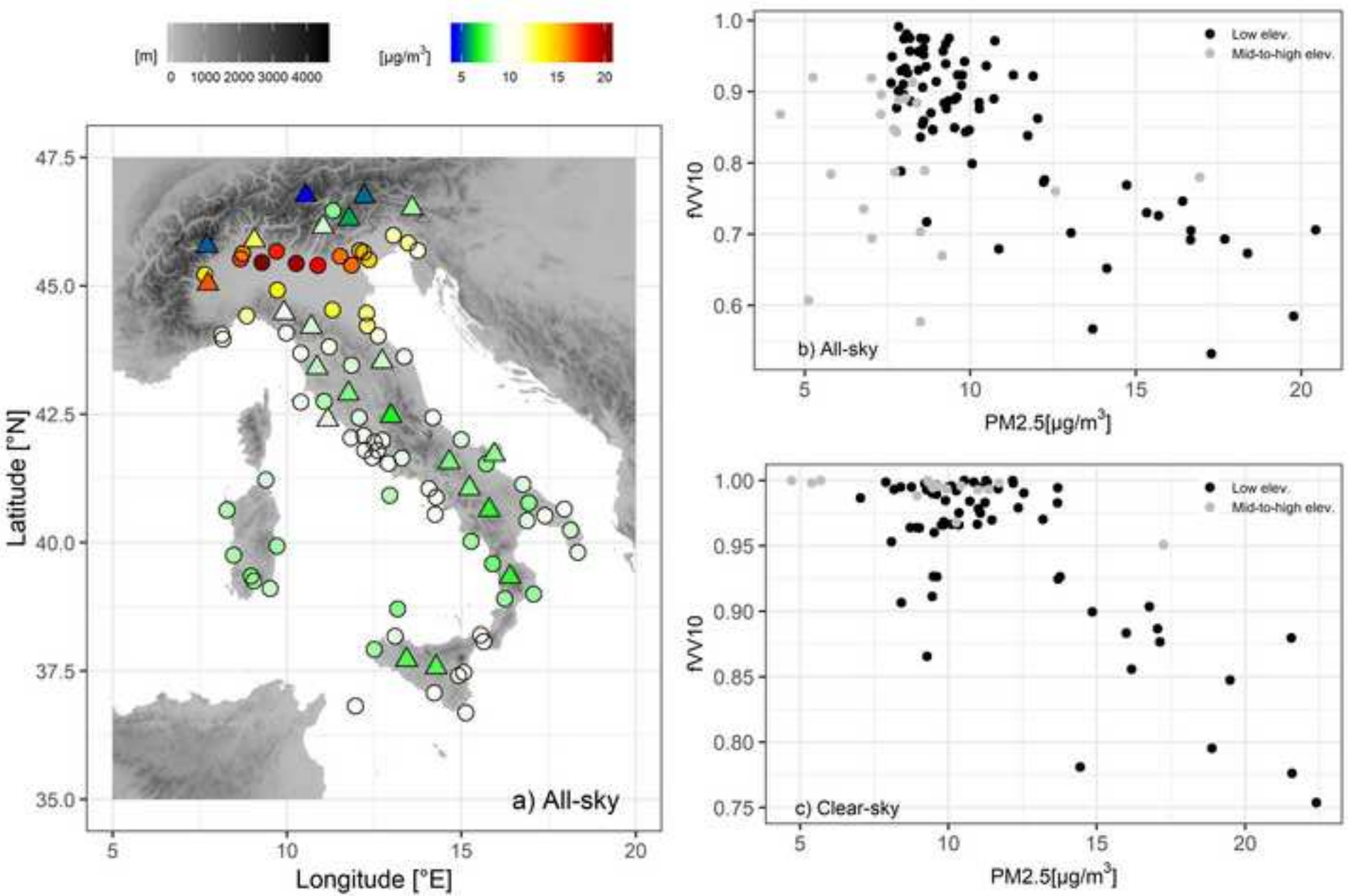

Figure 10

Click here to download high resolution image

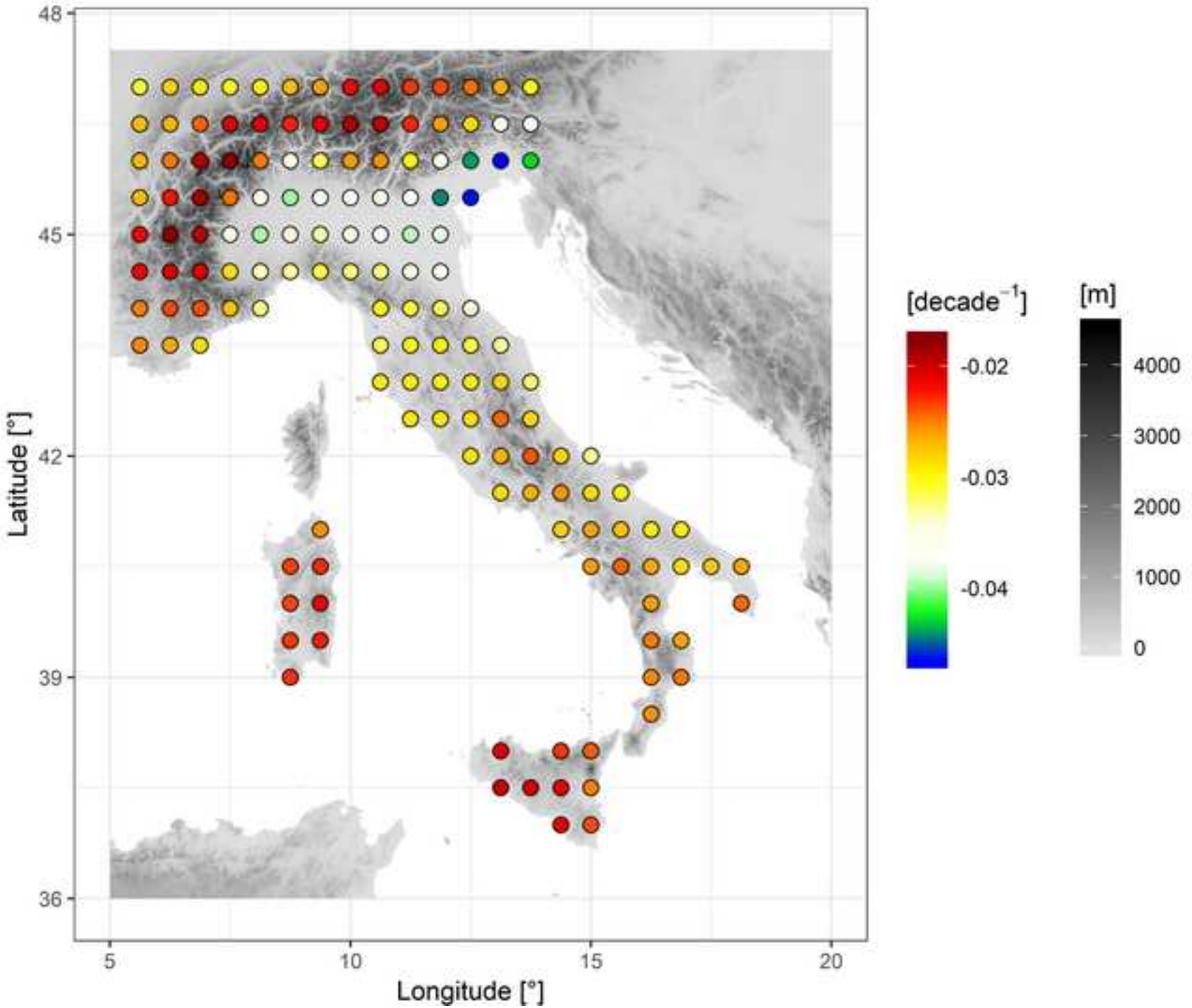

Figure 11

Click here to download high resolution image

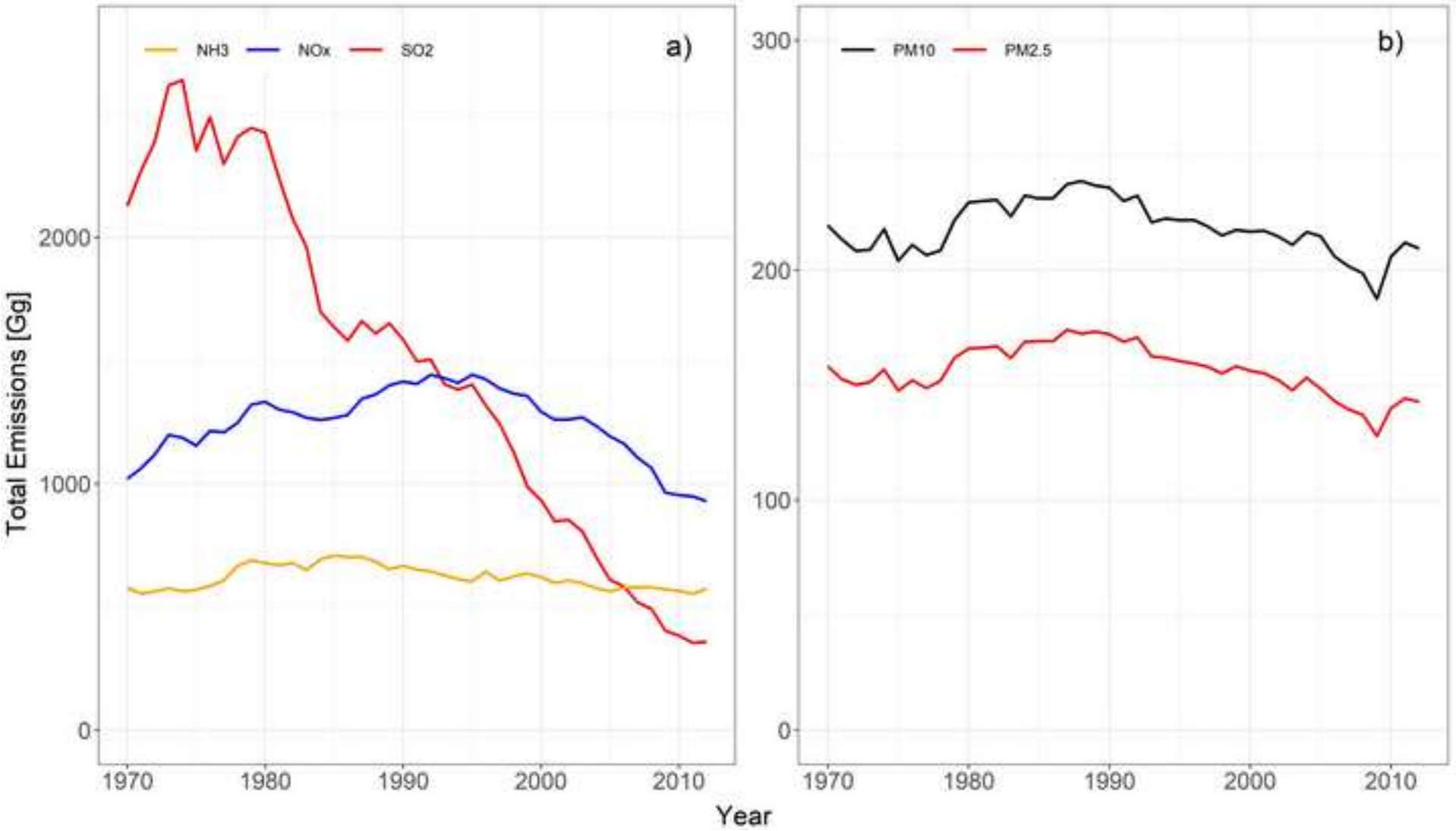

Highlights

- New data set of Italian quality/homogeneity checked visibility records
- 1951-2017 fraction of days with visibility higher than or equal to 10 km and 20 km
- Visibility records show a positive trend over the whole considered period
- Trends become weaker increasing the elevation
- The main driving factor seems to be aerosol load

***Declaration of Interest Statement**

Declaration of interests

☒ The authors declare that they have no known competing financial interests or personal relationships that could have appeared to influence the work reported in this paper.

☐The authors declare the following financial interests/personal relationships which may be considered as potential competing interests: